Hindawi
Advances in Civil Engineering
Volume 2018, Article ID 3976505, 15 pages
https://doi.org/10.1155/2018/3976505

Research Article

Increasing Permeability of Coal Seam and Improving Gas Drainage Using a Liquid Carbon Dioxide Phase Transition Explosive Technology

Wenrui He,[1,2,3] **Fulian He**,[1] **Kun Zhang**,[2,3] **Yongqiang Zhao**,[1] **and Hengzhong Zhu**[1]

[1]*College of Resources and Safety Engineering, China University of Mining and Technology, Beijing 100083, China*
[2]*School of Mines, China University of Mining and Technology, Xuzhou, Jiangsu 221116, China*
[3]*State Key Laboratory of Coal Resource and Safe Mining, Xuzhou, Jiangsu 221116, China*

Correspondence should be addressed to Wenrui He; 1522331579@qq.com

Received 30 April 2018; Revised 1 July 2018; Accepted 15 July 2018; Published 27 August 2018

Academic Editor: Dengke Wang

The low permeability of coal seams makes gas drainage difficult in lots of coal mines. This study presents a low-temperature, safe, and efficient liquid carbon dioxide phase transition explosive technology (LCDPTET) to increase the permeability of coal, thereby improving the efficiency of gas drainage and eliminating the dangers of coal and gas outburst. Meanwhile, an integrated approach for experimental determination, numerical simulation, and field testing was applied to study the damage ranges of coal and to determine a reasonable spacing between the gas drainage hole and blast hole. A numerical simulation model of liquid carbon dioxide phase transition explosion (LCDPTE) was built, and the damage index M was introduced to analyze the degree and range of coal damage after explosion at different spacings between the blast hole and the gas drainage hole. Furthermore, another aim was the assessment of the permeability changes and comparison of the gas drainage effects of different borehole spacings. The results showed that as the borehole spacing became smaller, the degree of coal damage around the gas drainage hole increased, and the gas drainage effect improved. However, to avoid the collapse of the gas drainage hole, the gas drainage holes should not be located in the crushing zone caused by LCDPTE. Based on the numerical analysis conducted to guide the borehole arrangement of the field test, the latter was carried out to study the increasing ranges of permeability of coal and the drainage effect after explosion. The results indicated that LCDPTET could greatly improve the permeability of the coal seam and gas drainage efficiency. In addition, this new technology could not only improve the safety and efficiency of mine production but could also turn carbon dioxide into an effective energy source worthy of popularization and application.

1. Introduction

Gas disasters have been a major factor threatening the safe and efficient production of mines during coal mining [1, 2]. Predrainage of coal seam gas is a method to control gas disasters, but coal seams in a lot of mines have low permeability, high ground stress, and difficulty in gas drainage [3–8]. To solve the above problems, scientists have conducted extensive and long-term explorations and practices; the methods used to improve the permeability of coal seams include mining protective coal seam, hydraulic fracturing, hydraulic slotting, deep-hole blasting, and microwave radiation are proposed [9–16]. Mining protective coal seams is suitable for combined drainage of multiple coal seams, but is limited to a single coal seam or a currently mined coal seam. Hydraulic fracturing and hydraulic slotting technologies used to increase the permeability of coal cause secondary pollution to coal seams, and the water consumption is tremendous. Deep-hole blasting is effective at increasing the permeability of coal seams, but the processes of implementation are dangerous. Microwave radiation technology is still at the experimental and developmental stages, and field applications require additional time. Therefore, it is crucial to find a technology to improve the permeability of coal seams.

The cardox tube system was first developed and used by a British company called CARDOX. Singh [17] found out

that the effects of two liquid carbon dioxide tubes combined explosion were same as five ordinary explosive tubes in Bulawayo gold mine test; he presented that liquid carbon dioxide phase transition explosive technology (LCDPTET) had the advantages of high safety and ecofriendly process and had no evacuation of equipment and operators in the process of blasting. The LCDPTET was similar to propellant fracturing technology [18, 19]; the high-pressure gas acted on the blasting medium to break the rock and increase its permeability. But it was different from propellant fracturing that generated high-temperature and high-pressure gases by combustion of propellant; the LCDPTET used a special explosive tube to heat and gasify liquid carbon dioxide, causing the liquid carbon dioxide to undergo a phase transition in a short time and generate the huge expansive pressure. The LCDPTET was applied to slope blasting, earthwork, and roadway excavation at an early stage [20, 21]. Because of its safe and efficient characteristics, scientists began to introduce it into the coal industry and use it to increase coal seam permeability at the end of the 20th century. Du et al. [22] systematically introduced equipment and technologies for the use of liquid carbon dioxide phase transition explosion (LCDPTE) in underground mines. Sun et al. [23] studied the failure law of coal via explosion of critical carbon dioxide and built a gas dynamics model. Chen et al. [24] conducted field tests of LCDPTE and concluded that liquid carbon dioxide phase technology can effectively improve coal seam permeability. Based on numerical analysis, Sun and Wang [25] studied the effect of explosive pressure on crack propagation when LCDPTET was used to break rock. Wang et al. [26] compared and analyzed the failure and fracture characteristics of rock masses after hydraulic fracturing and critical carbon dioxide explosions; they discovered that hydraulic fracturing cut rock mass into blocks, whereas a lot of microfractures were produced in the rock by LCDPTET in addition to macrofractures.

At present, the researches on increasing the permeability of coal seam by LCDPTET are still in the initial stage, and the related results are relatively less. Therefore, based on the background of a coal mine in Qianxi county in the Guizhou province of China, this paper conducted research on the LCDPTET. Section 2 of this paper introduces the principles, equipment, techniques, and advantages of LCDPTET for field applications in high-gas and low-permeability coal seams. In Section 3, the geological and mining conditions are analyzed, and gas and stratum parameters are determined to provide basic data for numerical simulations. In Section 4, the degrees of coal seam damages caused by LCDPTE and the gas drainage effects at different spacings between the gas drainage hole and the blast hole are numerically investigated in detail. In Section 5, based on the outcomes of numerical analyses, field investigations are performed to analyze the increasing ranges of permeability and optimum spacing of boreholes.

2. Principle and Technology of LCDPTE

2.1. Principle of LCDPTE. LCDPTET is a new physical explosive technology used to increase the permeability of coal seams, and it consists of three parts: filling, propulsion, and explosive systems. High-pressure gas that is produced by liquid carbon dioxide acts on the coal body around the borehole to crack coal and generate fractures. This increases the permeability of coal seams and gas migration channels, reduces the gas contents in coal seams, and prevents gas outburst.

LCDPTET has many advantages, mainly reflected in the following aspects: First, the gasification process of liquid carbon dioxide has the effect of cooling, and carbon dioxide is an inert gas. Therefore, it could prevent gas explosion or combustion accidents in the process of blasting operations, and it is especially suitable for the mines which are high in gas content or associated with dangers of coal and gas outbursts. At the same time, carbon dioxide gas could dilute methane to decrease the gas concentration in mines. Second, it is relatively safe to deal with the explosive tubes that did not work. Third, there is no toxic gas, the operation produces less dust, and there are no ill-effects on the health of the workers. Fourth, it has the advantages of low cost, simple operation, rapid filling, and high production efficiency.

2.2. LCDPTE Technology

2.2.1. Filling System. The filling system consists of a liquid carbon dioxide storage tank, a gas compressor, a flowmeter, a refrigerator, and CO_2 explosive tubes. The gas compressor is the main power device used to inject liquid carbon dioxide into the explosive tubes. The flowmeter monitors the liquid carbon dioxide flow from storage tank to the CO_2 explosive tubes. As the liquid carbon dioxide is easily converted into gas at normal or high temperatures, a refrigerator is installed in the pipeline to reduce the temperature in the conveying pipe. Considering the comprehensive economic benefits and explosive efficiency, liquid carbon dioxide with a purity of 99.9% is usually used in engineering. The filling system is shown in Figure 1.

2.2.2. Explosive System. The explosive system is the core of LCDPTET, which consists of a drill pipe, an explosive tube, a liquid CO_2 storage chamber, a constant-pressure shearing disc, and a gas release tube. High-pressure gas is ejected from the gas ports at specific directions and angles in the gas release tube and acts on the coal body around the blast hole. The direction and diameter of the gas ports are designed to control the gas flow direction and concentrate the energy according to common engineering practices. The liquid CO_2 storage chamber is used for storing liquid carbon dioxide and has high strength and corrosion resistance. One end of the chamber is equipped with a constant-pressure shearing disc, and the other end is connected to an explosive tube and a liquid injection head. The explosive in the explosive tube is similar to the propellant in high-energy gas-fracturing technology [27]; when the circuit in the explosive tube passes a current of 0.8 A or more, the explosive burns and emits a lot of heat, heating and gasifying the liquid carbon dioxide. The reaction time is about 1–20 ms [28]. The constant-pressure shearing disc installed between the liquid storage chamber and gas release tube is made of steel having

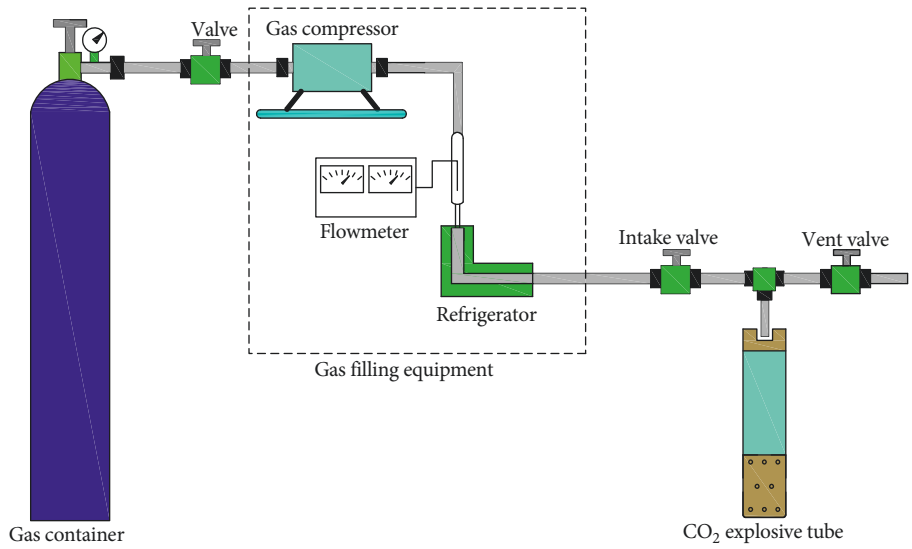

Figure 1: Filling system.

a specific strength, and it is used to control the gas pressure during explosion. When the pressure produced by the phase transition of the liquid carbon dioxide in the storage tank is greater than the maximum failure pressure of the shearing disc, the disc will be broken and high-pressure carbon dioxide gas will rush into the release tube. The maximum breakdown pressure of the constant-pressure shearing disc is in the range of 126–276 MPa according to engineering requirements. After the start-up of the explosive device, the transition process of liquid carbon dioxide to gas will last for approximately 20 ms. Therefore, the explosive gas pressure is approximately equivalent to the maximum breakdown force of the constant-pressure shearing disc [29]. The explosive system is shown in Figure 2.

2.2.3. Propulsion System. The propulsion machine can safely and accurately send the explosive tubes to the blasting location through the borehole and retrieve them after the explosion. Figure 3 shows the propulsion system.

3. Case Study

3.1. Geological and Mining Conditions. This case study focuses on a coal mine located in Qianxi county in the Guizhou province of China (Figure 4). It is a coal and gas outburst mine, and the current mining seam is #17. The average overburden depth and thickness of the coal seam are 180 and 2.5 m, respectively. The roof and floor of coal seam are sandy mudstone and mudstone, and their thicknesses are 3 m and 1.7 m, respectively. The permeability of the #17 coal seam is low, and the gas concentrations often exceed a safety margin, thus leading to occurrences of gas dynamic disasters during excavation. Therefore, LCDPTETs operated in floor rock roadways are applied to increase the permeability through boreholes which penetrate the #17 coal seam. The measurements of predrainage of coal strip gas are then obtained to reduce the gas pressures and contents of coal seams and eliminate the dangers of coal and gas outbursts.

The floor rock roadway is located under the mudstone layer of the floor of the #17 coal seam. The average vertical distance from the roof of roadway to the coal seam is 15 m. The section shape of the roadway is rectangular; the height and width of the roadway are 2.5 and 3.5 m, respectively. The strike length of the test area is 60 m. The locations of the floor rock roadway and the test area are shown in Figure 5.

3.2. Laboratory Tests. To better understand the increase of the permeability ranges of coal seams after LCDPTE and to achieve a reasonable spacing between the gas drainage hole and the blast hole, laboratory tests were carried out on rock and coal samples collected from the floor rock roadway of the 11703 working face to determine the mechanical properties of the rock and porosity, permeability, ash content, moisture content, and adsorption constant of the coal seam.

3.2.1. Experimental Determination of the Mechanical Properties of Rock. Tests were conducted on a servo-controlled system (TAW–2000); its maximum axial load was 2000 kN, maximum shear load was 500 kN, and maximum lateral load was 500 kN. The uniaxial compressive strength, Young's modulus, and Poisson's ratio were obtained by conducting uniaxial compression tests. Four samples were tested for each lithology, namely, the roof, coal seam, and floor. Based on the results of these tests, the mechanical parameters of each geological unit are shown in Table 1.

3.2.2. Parameters of Coal Seams. The porosities of eight coal samples were determined by Mercury intrusion methods. The permeabilities of four of the samples were tested using a U–MPB–1 gas permeability tester with occupation standard (SY/T 5336–2006) [30]. Gas adsorption constants of five of the coal samples were tested by the high-pressure isothermal adsorption test method (GBT–19560–2008) [31]. The eight sets of coal samples were tested using a coal quality analyzer. The measured data are shown in Table 2.

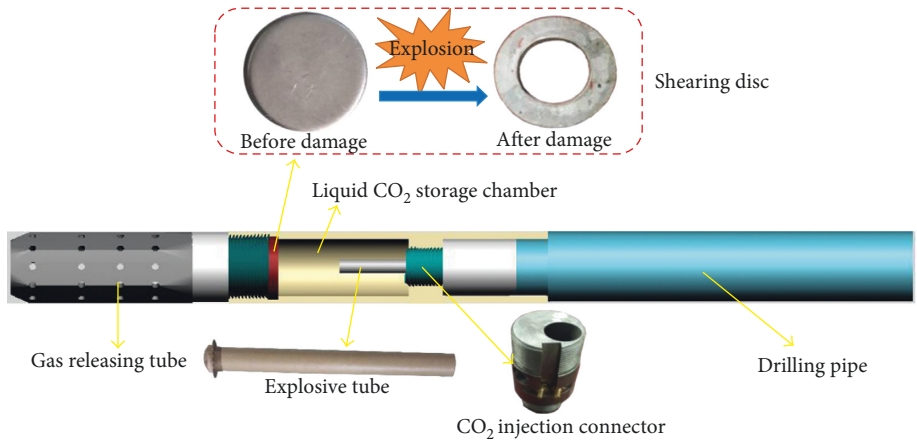

Figure 2: Explosive system.

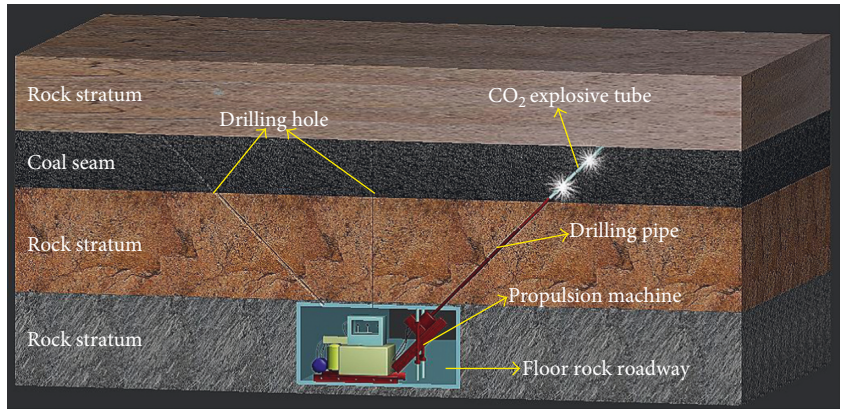

Figure 3: Propulsion system.

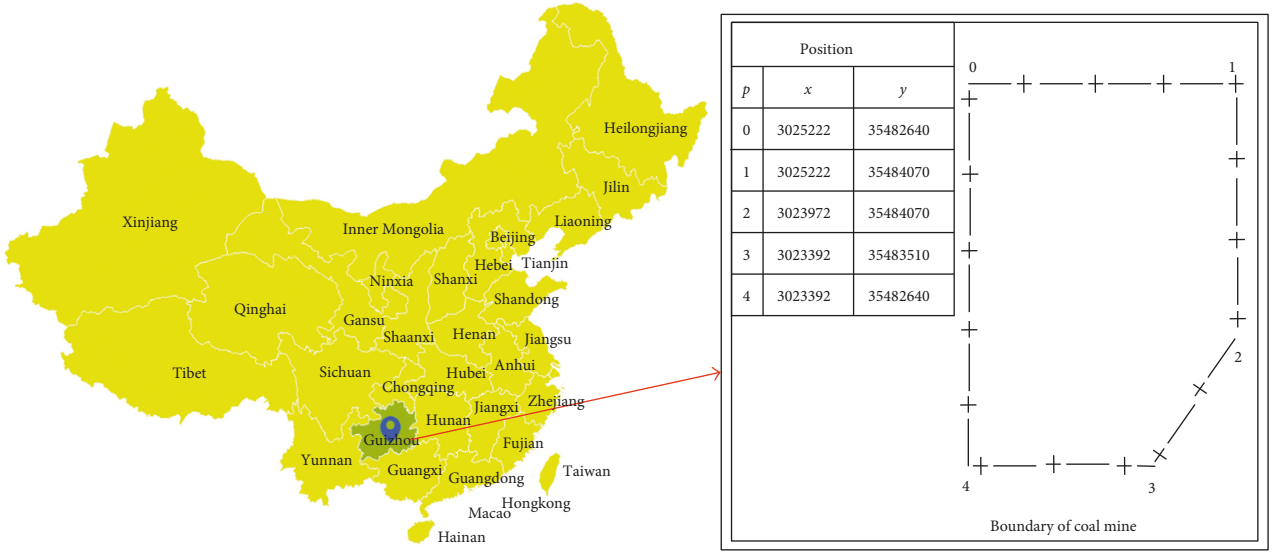

Figure 4: Location of test size.

3.3. In Situ Measurement. According to the direct method of determining coal seam gas content (GB/T 23250–2009) [32], the original gas content of 15 coalbed samples were obtained using a gas desorption velocity measuring instrument. According to the direct measurement methods of the coal seam gas pressure in mines (AQ/T 1047–2007) [33], adopting

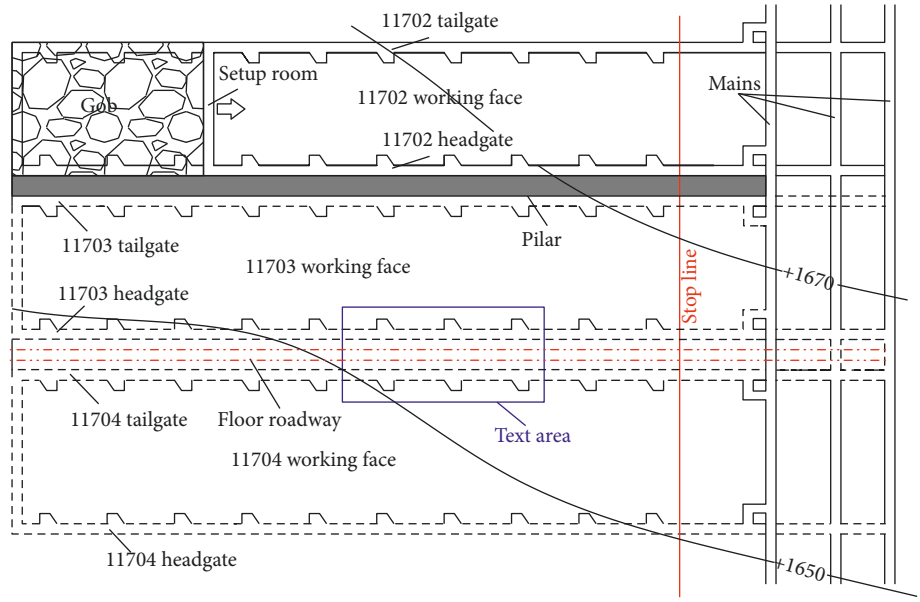

Figure 5: Location of test area.

Table 1: Mechanical properties of each geological unit.

Lithology	Modulus of elasticity E (GPa)	Uniaxial compressive strength σ_c (MPa)	Uniaxial tensile strength σ_t (MPa)	Poisson's ratio v	Friction angle ϕ (°)
Sandy mudstone	17.3	31.1	2.45	0.23	32
Coal	5.2	13.6	1.68	0.3	29
Mudstone	11.4	25.3	1.87	0.29	30

Table 2: Coal seam parameters.

Gas contents (m^3/t)	Maximum relative pressure of gas (MPa)	Porosity	Permeability (m^2)	Adsorption constant a (m^3/kg)	Adsorption constant b (MPa^{-1})	Ash content (%)	Moisture content (%)
10.6	0.98	0.065	3.9×10^{-16}	14.5	0.75	0.14	0.04

passive pressure methods can measure the gas pressure of the coal seam effectively. The measurement data are shown in Table 2.

4. Numerical Analysis of Increasing Permeability Ranges and Gas Drainage Effect

The degrees of coal damage after LCDPTE were numerically analyzed, and the gas drainage after increasing the permeability of the coal seam was evaluated to study the optimum spacing between the drainage hole and the blast hole. This could provide a basis and guidance for field tests.

4.1. The Principle of Numerical Analysis

4.1.1. Governing Equation of Stress and Deformation. The effective stress equation embodies the coupling of gas-solid stress:

$$\sigma_{ij} = 2G\varepsilon_{ij} + \lambda\delta_{ij} - \alpha\delta_{ij}p, \tag{1}$$

where σ_{ij} is the coal stress component, ε_{ij} is the strain component, λ and G are the Lame constants given by $\lambda = Ev/(2(1+\mathrm{v}))$ and $G = E/(2(1+\mathrm{v}))$, respectively, δ_{ij} is the Kronecker symbol, p is the gas pressure, and α is the Biot's coefficient, which is determined by the compressibility of the coal.

The equation that governs stress is

$$Gu_{i,ij} + \frac{G}{1-2v}u_{j,ji} + \alpha p_i + F_i = 0, \tag{2}$$

where G is the shear modulus, v is the Poisson's ratio, F_i is the component of the body force in the ith direction, and u_i is the component of the displacement in the ith direction.

Equivalently, the strain expression is

$$\varepsilon_{ij} = \frac{1}{2}\left(u_{ij} + u_{ji}\right), \tag{3}$$

where u_{ij} and u_{ji} are the coal displacement components.

4.1.2. Coal Damage Governing Equation. In this study, the maximum tensile stress criterion was used to judge the tensile failure, and the Mohr–Coulomb criterion was used to judge shear or compression failure. The coal damage expression is

$$F_t = -\sigma_3 - \sigma_{t0}, \tag{4}$$

$$F_c = \sigma_1 - \sigma_3 \frac{1+\sin\phi}{1-\sin\phi} - \sigma_{c0}, \tag{5}$$

where σ_{c0} is the uniaxial compressive strength, σ_{t0} is the uniaxial tensile strength, and F_t and F_c are the functions that represent the stress states. When the values of these functions are 0, as shown in (6), the coal is subjected to tensile and shear failures, respectively; ϕ is the friction angles; σ_1 and σ_3 are the maximum and minimum principal stresses, respectively.

$$\begin{aligned} F_t &= 0 \\ \text{or } F_c &= 0. \end{aligned} \tag{6}$$

When the coal stresses meet the maximum tensile stress criterion, tensile failure will occur. Conversely, when the stresses meet the Mohr–Coulomb criterion, compression or shear failure will occur. Compared with shear and compression failures, the tensile strength of coal is the smallest in rock mechanics. Therefore, tensile failure is identified as a priority damage criterion in the rock failure category.

Index M_i indicates the degree of coal damage and is expressed as [34]:

$$M_i = \begin{cases} 0, & F_t < 0,\ F_c < 0, \\ 1 - \left|\frac{\varepsilon_{t0}}{\varepsilon_3}\right|^2, & F_t = 0,\ dF_t > 0, \\ 1 - \left|\frac{\varepsilon_{c0}}{\varepsilon_1}\right|^2, & F_c = 0,\ dF_c > 0, \end{cases} \tag{7}$$

where ε_{t0} is the maximum tensile strain at tensile failure, ε_{c0} is the maximum compressive strain at compression failure, ε_1 is the maximum principle strain, and ε_3 is the minimum principle strain. The expressions $dF_t > 0$ and $dF_c > 0$ indicate the load state where two types of failures might occur and cause a continuous increase of index M_i. Equivalently, $dF_t < 0$ or $dF_c < 0$ indicates the unloaded state where new coal damages are not produced, and the values of index M_i remain unchanged.

The elastic modulus of coal is given based on the elastic failure theory and is expressed as

$$E_i = (1 - M_i)E_0, \tag{8}$$

where E_0 and E_i are the elastic moduli before and after failure, respectively. In this study, the failure and its further evolution occur in an isotropic medium; therefore, E_i, E_0, and M_i are scalars.

4.1.3. Gas Seepage Equation. The porosity of coal [35] is given by

$$\varphi = 1 - \frac{1-\varphi_0}{1+\varepsilon_v}\left(1 - \frac{p-p_0}{K_s}\right), \tag{9}$$

where φ is the porosity, φ_0 is the initial porosity, ε_v is the coal volume strain, p_0 is the gas' initial pressure in the coal seam, and K_s is the volume compression modulus of coal.

The permeability of coal can be obtained under an isothermal condition based on the Kozeny–Caman equation of seepage mechanics,

$$k_1 = \frac{k_0}{1+\varepsilon_v}\left(p + \frac{\varepsilon_v}{\varphi_0} + \frac{(p-p_0)(1-\varphi_0)}{\varphi_0 K_s}\right), \tag{10}$$

where k_1 is permeability of coal, and k_0 is the initial permeability of coal.

The permeability after damage [36] is expressed as

$$k_2 = k_1 e^{M_i}, \tag{11}$$

where k_2 is the permeability after damage.

Additionally, the gas seepage equation [37] is given by:

$$\frac{\partial \varphi}{\partial t} p + \left(\varphi + \frac{ab\rho_c(1-A-B)}{(1+bp)^2}\right)\frac{\partial p}{\partial t} = \nabla\left(\frac{k}{\mu}\left(1 + \frac{m}{p}\right)\nabla p^2\right), \tag{12}$$

where t is the time, a and b are the gas adsorption constants, μ is the viscosity of methane gas, m is the Klingberg coefficient, A is the ash content, and B is the moisture content.

4.1.4. The Principle of Numerical Calculation. The numerical model in this study used a finite element method to solve the control equation. The elastic failure model and the fluid-solid coupling model of gas flow were used to simulate the process of LCDPTE and the gas drainage after explosion, respectively. The process of numerical calculation was shown in Figure 6.

The specific steps were as follows:

Step 1. Based on (1)–(3), the stress σ_{ij} and strain ε_{ij} of the coal were calculated when the gas impact pressure P_1 was applied to the boundary of the blast hole at the initial time.

Step 2. Based on the results obtained in the first step, the maximum principal stress σ_1 and the minimum principal stress σ_3 in the coal body were obtained, then according to the (4)–(6) to determine whether the coal body was damaged.

Step 3. When the coal body was damaged, the maximum principal strain ε_1 and the minimum principal strain ε_3 in the coal body were determined from the results obtained in the first step, and the damage index M_1 was obtained according to (7).

Step 4. The damage index M_1 was plugged into (8), and the modified elastic modulus E_1 was obtained after coal failure, and it participated in the calculation of the next cycle.

Step 5. The gas impact pressure at the next moment P_2 was applied to the boundary of the blast hole and cycled from the first step to the fourth step until the gas impact pressure P_i is 0 MPa.

Step 6. The final damage index M_i was plugged into (11) to determine the permeability of coal after explosion.

Step 7. Gas drainage pressure was applied to the gas drainage hole. The dynamic process of gas drainage was determined by the (1), (9), (10)–(12).

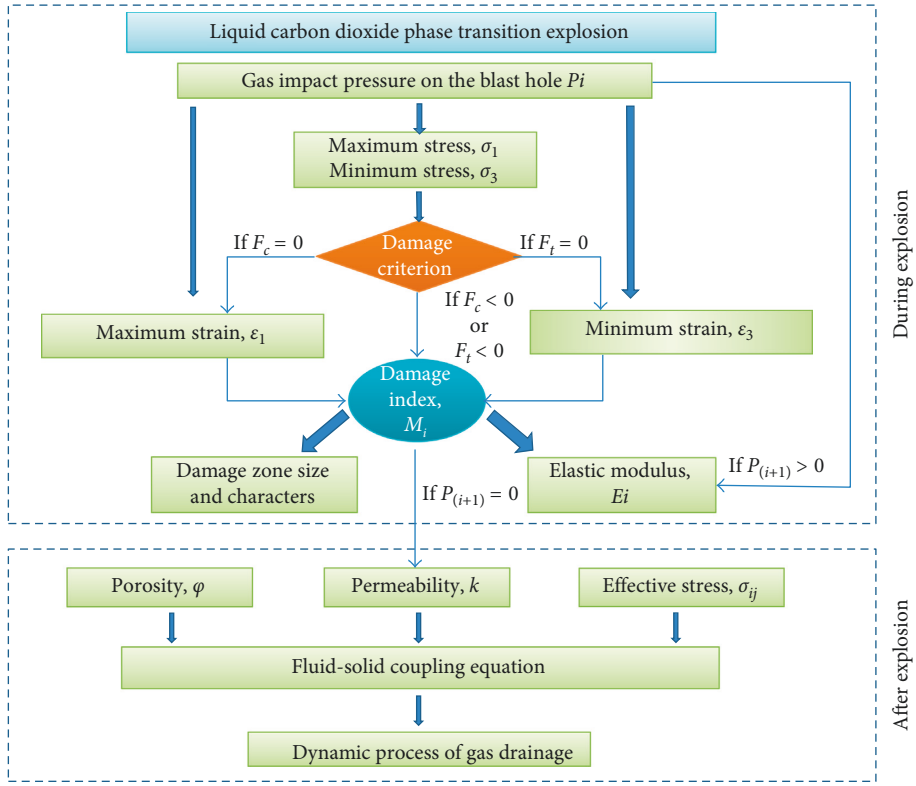

Figure 6: Process of numerical calculation.

4.1.5. Model Verification. Based on the relevant parameters in literature [38], the abovementioned fluid-solid coupled numerical model was used to analyze the gas radial flow rate in the coal body under steady flow. And the numerical solutions were compared with the test data in the literature [38] to verify the accuracy of the model used in the study and finite element calculations.

Figure 7 presents the comparison of test data and simulation results of gas radial percolation rate. It can be observed from Figure 7 that the simulation results are in good agreement with the test data, indicating that the numerical model used in this study and its finite element calculation are reasonable and reliable.

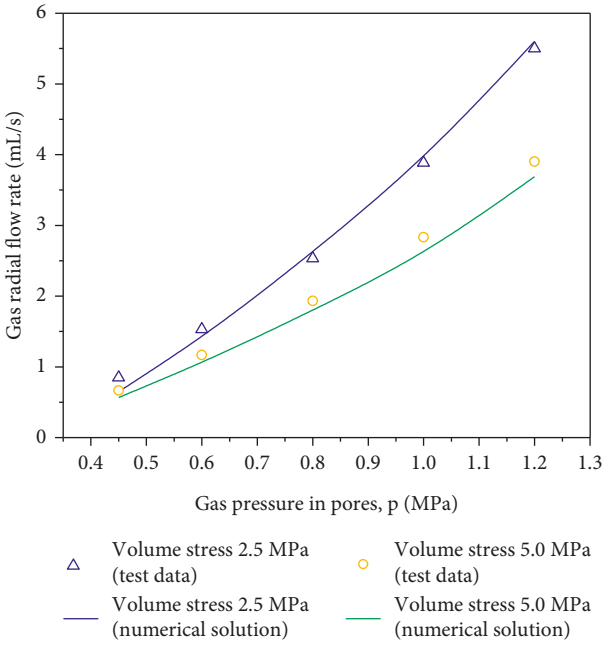

Figure 7: Comparison of test data and simulation results of gas radial flow rate.

4.2. Numerical Model Generation

4.2.1. Numerical Simulation Model and Simulation Plan. The coal seam, roof, and floor were established in the model, and their dimensions were $3 \times 20 \times 20$ m, $2.4 \times 20 \times 20$ m, and $1.8 \times 20 \times 20$ m, respectively, as shown in Figure 8(a). In order to determine the increasing permeability ranges of coal after LCDPTE and reasonable borehole spacing, various plans at 3, 4, 5, and 6 m spacings between the gas drainage hole and the blast hole were carried out in this study. A blast hole was located at the center of the model and vertically penetrated the coal seams from the floor. Its coordinates were ($x = 10$, $y = 10$), and the hole depth was 4.2 m. The coordinates of the gas drainage holes of the four plans were ($x = 10$, $y = 13$), ($x = 10$, $y = 14$), ($x = 10$, $y = 15$), and ($x = 10$, $y = 16$). These coordinates are the same for the blast holes, which vertically penetrate the coal seams from below, and the borehole depths are all 4.2 m, as shown in Figure 8(b). The diameters of the blast holes and gas drainage holes are 100 mm.

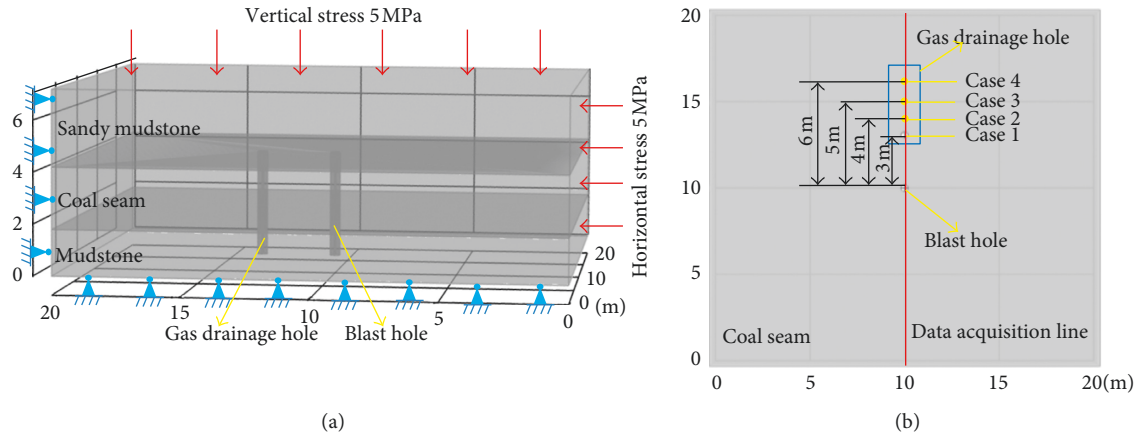

Figure 8: Numerical simulation model: (a) three-dimensional model; (b) top views.

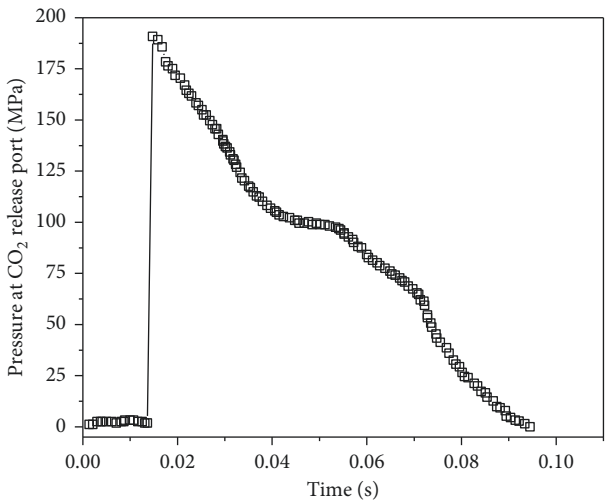

Figure 9: Change of pressure over time at the CO_2 gas release port.

4.2.2. Initial and Boundary Conditions. The initial gas pressure in the coal seam was 2 MPa. The gas impact pressure produced by liquid carbon dioxide phase transition applied to the boundary of blast hole was obtained from the tests, and the values of impact pressure changed over time, as shown in Figure 9. The negative pressure of gas drainage (5×10^{-3} MPa) was applied to the boundary of the gas drainage hole. A vertical stress (5 MPa) was applied to the top of the model, a horizontal stress (5 MPa) was applied to its right and posterior sides, and roll supports were applied to the left, front, and bottom sides.

4.2.3. Simulation Parameters. A reasonable parameter setting is crucial to ensure the accuracy of the numerical analysis. The stiffness of the numerical analysis model recommended by Mohammad et al. [39] should be equal to 0.47 times the average stiffness value obtained from the laboratory tests. Cai et al. [40] suggested that the elastic modulus and uniaxial compressive strength of coal and rock masses can be in the range of 0.1–0.25 times that of the values of the laboratory tests, while the Poisson's ratio is assumed to be in the range of 1.2–1.4 times that of the values of the laboratory tests. Therefore, the elastic modulus, compressive strength, and tensile strength of coal and rock masses are equal to 0.25 times that of the values of the laboratory tests, whereas the Poisson's ratio is 1.2 times that of the laboratory test values. The shear modulus is calculated from elastic modulus and Poisson's ratio. The porosity, permeability, ash content, moisture content, and adsorption constant of the coal seam are shown by the results in Table 2; the numerical simulation parameters are shown in Table 3.

Table 3: Numerical simulation parameters.

	Parameters	Values
Coal	Initial porosity φ_0	0.065
	Initial permeability k_0 (m^2)	3.90×10^{-16}
	Elastic modulus E (GPa)	1.30
	Kronecker symbol δ_{ij}	1.00
	Klingberg coefficient m (Pa)	7.60×10^5
	Poisson's ratio ν	0.36
	Shear modulus G (GPa)	0.52
	Ash content A	0.14
	Moisture content B	0.04
	Adsorption constant a (m^3/kg)	14.5
	Tensile strength σ_t (MPa)	0.42
	Compressive strength σ_c (MPa)	3.40
	Friction angle ϕ (°)	29
	Adsorption constant b (MPa^{-1})	0.75
	Coal density ρ_c (kg/m^3)	1400
	Biot coefficient	1
Sandy mudstone of roof	Tensile strength σ_t (MPa)	0.61
	Compressive strength σ_c (MPa)	7.78
	Friction angle ϕ (°)	32
	Elastic modulus E (GPa)	4.34
	Poisson's ratio ν	0.28
Mudstone of floor	Tensile strength σ_t (MPa)	0.47
	Compressive strength σ_c (MPa)	6.33
	Friction angle ϕ (°)	30
	Elastic modulus E (GPa)	2.85
	Poisson's ratio ν	0.35
Methane gas	Viscosity μ (Pa·s)	1.10×10^{-5}

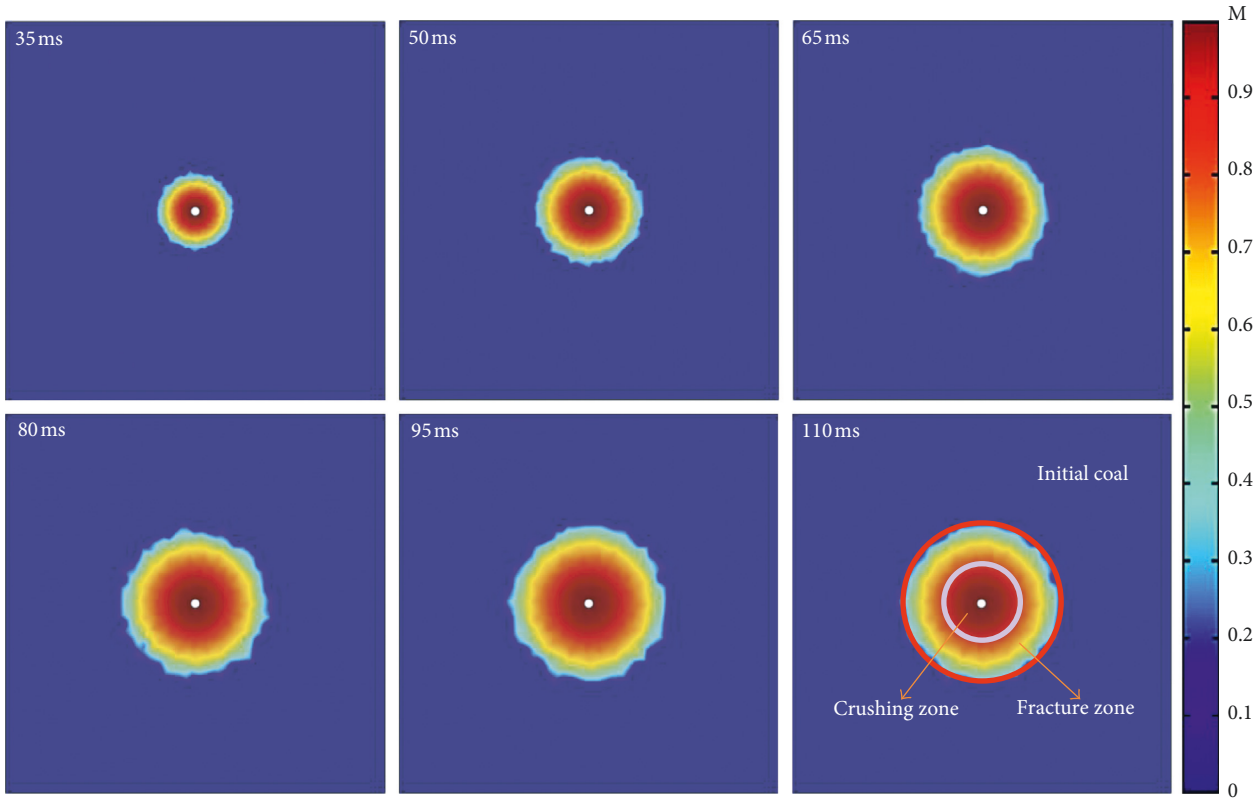

Figure 10: Expansion of damage zone over time.

4.3. Results and Analyses

4.3.1. Increasing Coal Permeability Ranges. Figure 10 shows the expansion of the damage zone over time during the explosion process. When the damage index M_i is greater than 0, it indicates that the coal body has been destroyed, so that the size of the coal damage zone can be identified. At the same time, the value of damage index M_i indicates the degree of coal damage, which can be used to represent the characteristics of the damage zone. Based on the study of degree of coal damage by Zhu et al. [41], the fracture zone ($0 < M < 0.7$) and crushing zone ($0.7 \le M \le 1$) are chosen according to the damage index M_i.

It can be observed from Figure 10 that the radius of damage zone is 1.91, 3.04, 3.88, 4.33, 4.56, and 4.56 m at 35, 50, 65, 80, 95, and 110 ms, respectively. When time increases, the impact pressure of the explosion gas attenuates and the expansion rate of the damage zone decreases. At 95 ms, the damage zone expansion stops. The radius of the crushing zone determined by the damage index is approximately 2 m, and the radius of fracture zone ranges from 2 m to 4.56 m.

Figure 11 presents the numerical simulation results of coal permeability changes. The values of permeability are proportional to the height; the more the height, the greater is the permeability. At same time, Figure 11 shows enhanced permeability as maximum at the blast hole and decreasing radially away from the hole, and it was proved by the laboratory test results obtained by Chen and Zhou [42]. The high-pressure impact gas generated by the phase transition of liquid carbon dioxide will strongly compress the coal body, and the coal body around the blast hole will be compressed and damaged to form a crushing damage zone. Then, the high-pressure gas enters into the coal body through the fractures of the crushing zone and produces a splitting effect on the coal, which makes the coal body tensile damage and produces a lot of fractures, forming a fracture zone.

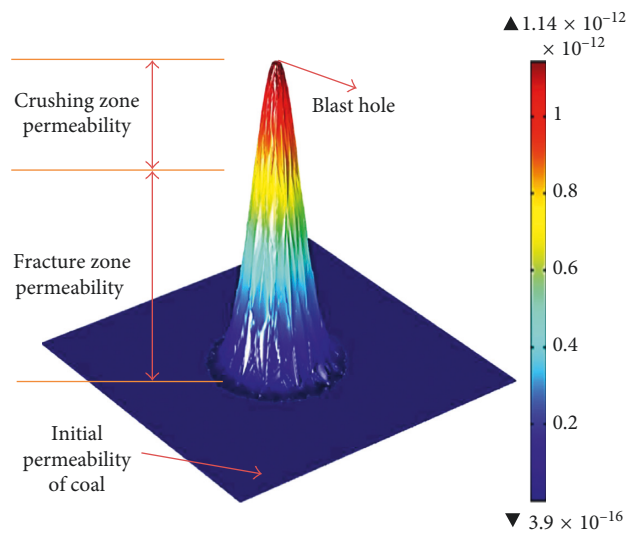

Figure 11: Coal permeability changes after the explosion.

It can be observed from Figure 11 that the original coal permeability is 3.9×10^{-16} m^2, the fracture zone permeability

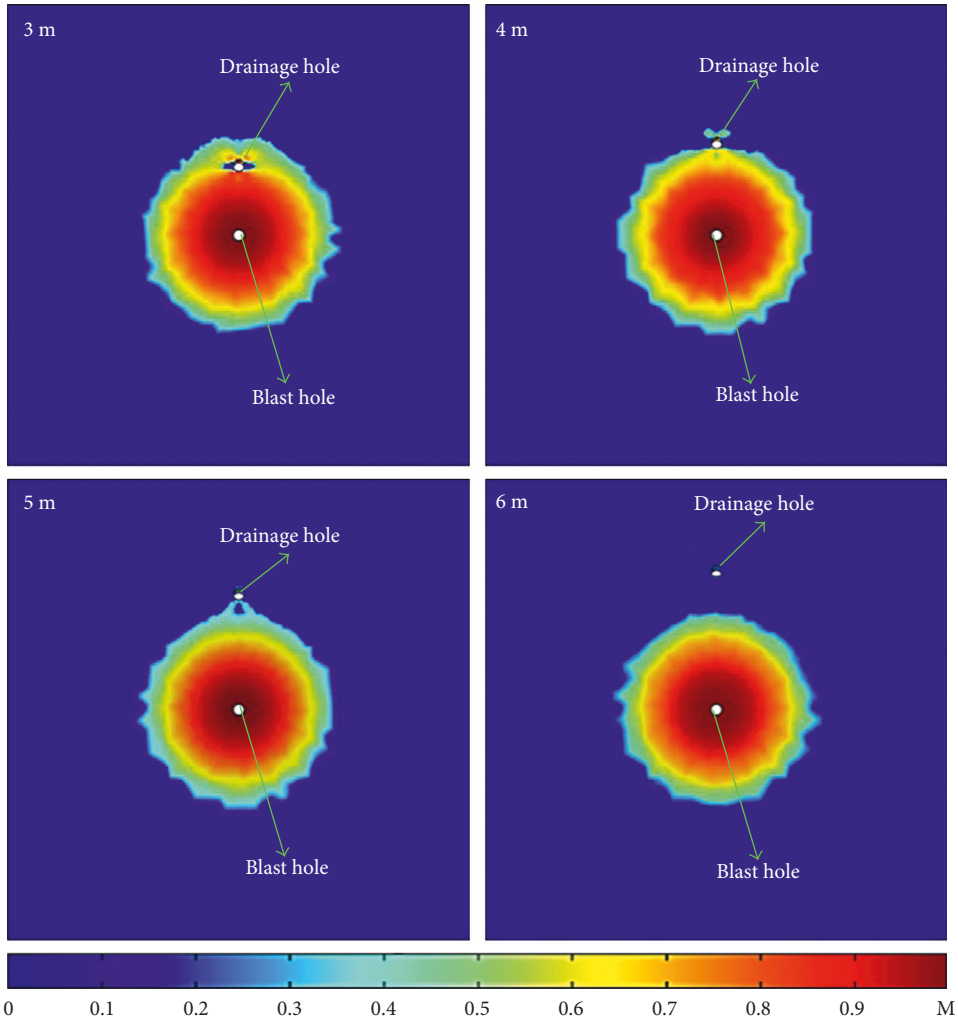

Figure 12: Degrees of coal damage and damage ranges for different borehole spacings.

is in range of 4.0×10^{-16}–7.2×10^{-13} m^2, and the crushing zone permeability is in the range of 7.2×10^{-13}–1.14×10^{-12} m^2. Therefore, the permeability of coal is greatly improved after LCDPTE; this provides space and channels for gas adsorption and migration, effectively reduces gas pressures in the coal seam, and improves the gas drainage efficiency.

Figure 12 presents the results of the degree of coal damages for different spacings (3, 4, 5, and 6 m) between the blast hole and the gas drainage hole. As shown in Figure 12, the gas drainage hole is located in the fracture zone when the spacing is 3 m, and the coal around the gas drainage hole will generate a lot of fractures, which increases the coal's permeability. The damage zone extends to the gas drainage hole when the spacing is 4 m, and a small fracture zone similar to a butterfly wing is produced on the side away from the blast hole. When the spacing is 5 m, the gas drainage hole is located at the edge of the fracture zone, and there is no coal damage on the other side of the gas drainage hole. When the spacing is 6 m, the damage zone after the explosion does not affect the coal around the gas drainage hole, and the permeability around the gas drainage hole remains unchanged. Thus, compared to the increasing permeability radius (4.5 m) of a single blast hole, when there is a gas drainage hole beside the blast hole, the increasing permeability radius is approximately 5 m because the gas drainage hole increases the free surface of deformation and expansion of coal during the explosion.

4.3.2. Gas Drainage Effects after Explosion. Based on the above analysis, gas drainage effects are further studied after the explosion to determine the reasonable spacing between drainage holes and blast holes; the spacings chosen are 3, 4, 5, and 6 m.

Figure 13 presents the results of gas drainage for 30 d after LCDPTE. Gas pressures in the coal begin to decrease from the zone where the permeability has been improved, as shown in Figure 13. When the spacing between the gas drainage hole and blast hole is 3 m, the fractures around the gas drainage hole connect with the crushing zone, which improves the permeability considerably. Therefore, after gas drainage over a period of 30 d, gas pressures in large areas of coal around the blast hole and the gas drainage hole are

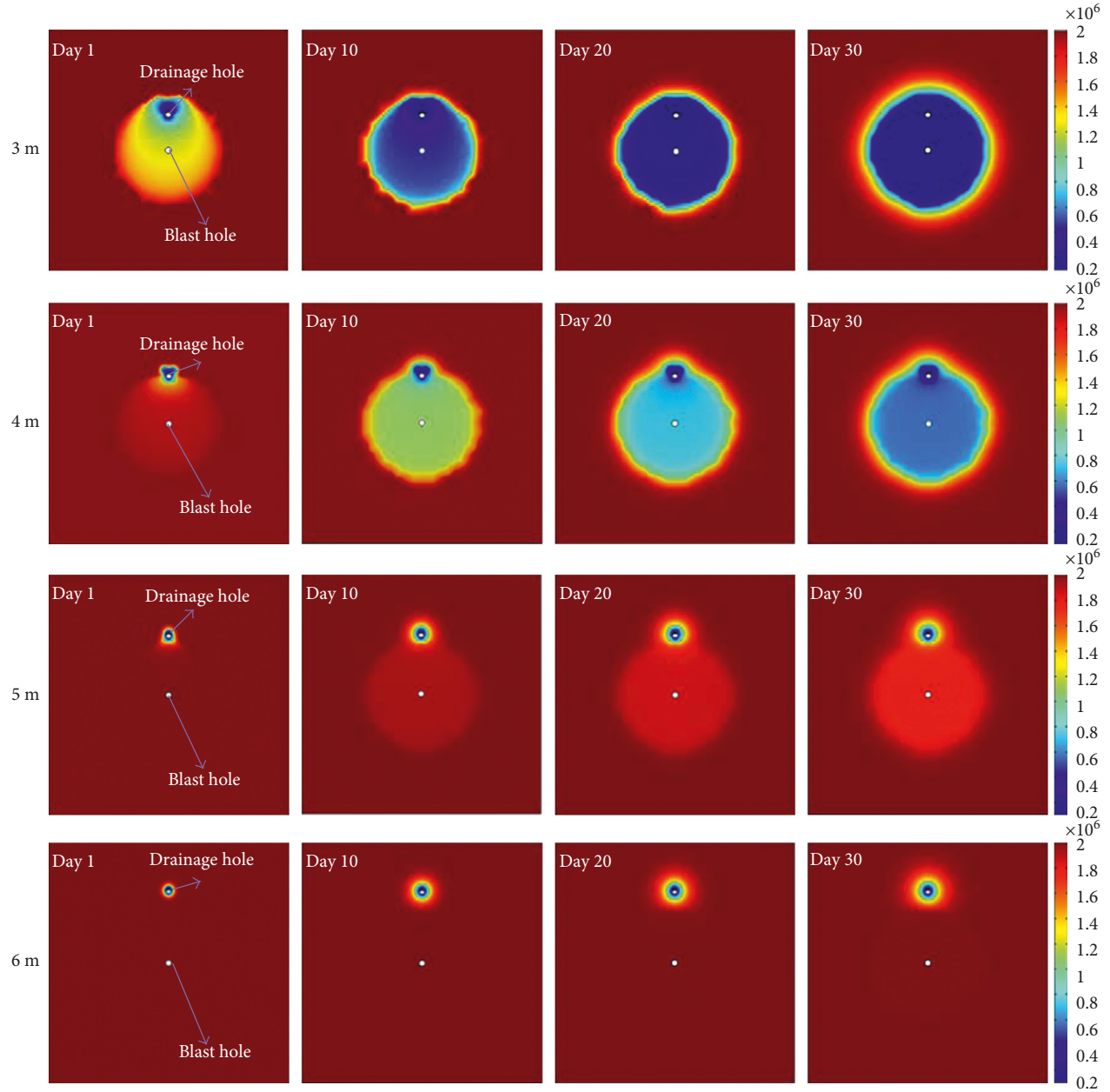

Figure 13: Gas drainage effects after explosion.

reduced to nearly 0 MPa. When the spacing is 4 m, gas pressures in large areas around the blast hole and the gas drainage hole are reduced over a period of 30 d, but the rates of decline are low. The gas drainage hole with 5 m spacing is at the edge of the fracture zone after explosion, and its connectivity with the fractures is less. However, after gas drainage for 30 d, only the gas pressures around the gas drainage holes are reduced, and any reductions around the blast hole are extremely small. The gas drainage hole with 6 m spacing is in the undamaged coal zone, and the permeability of coal around the gas drainage hole has not increased; therefore, the effects of gas drainage are the same as those without LCDPTE.

Figure 14 presents the relationships of gas pressure versus time for the four borehole spacing arrangements. As shown in Figure 14, the coal on the side of the gas drainage hole that is far from the blast hole is affected to a lesser degree by the explosion, and it is not in the zones where the permeability increases. Therefore, the decrease of the gas pressure in these zones is smaller as a function of the gas drainage time. When the spacing between the gas drainage hole and the blast hole is 3 m, the gas in the increasing permeability zones move faster and are fully drained after 1 d. Correspondingly, the gas pressures reduce to 1.25 MPa after gas drainage of 1 d, whereas after a gas drainage of 10 d, the gas pressures drop to 2.40×10^{-3} MPa, and the gas pressures approach 0 MPa when the drainage lasts for 20 d. Whereas for a gas drainage of 30 d, the gas pressures in the increasing permeability zones reduce to 0.47 and 1.69 MPa when the spacing between the gas drainage hole and the blast

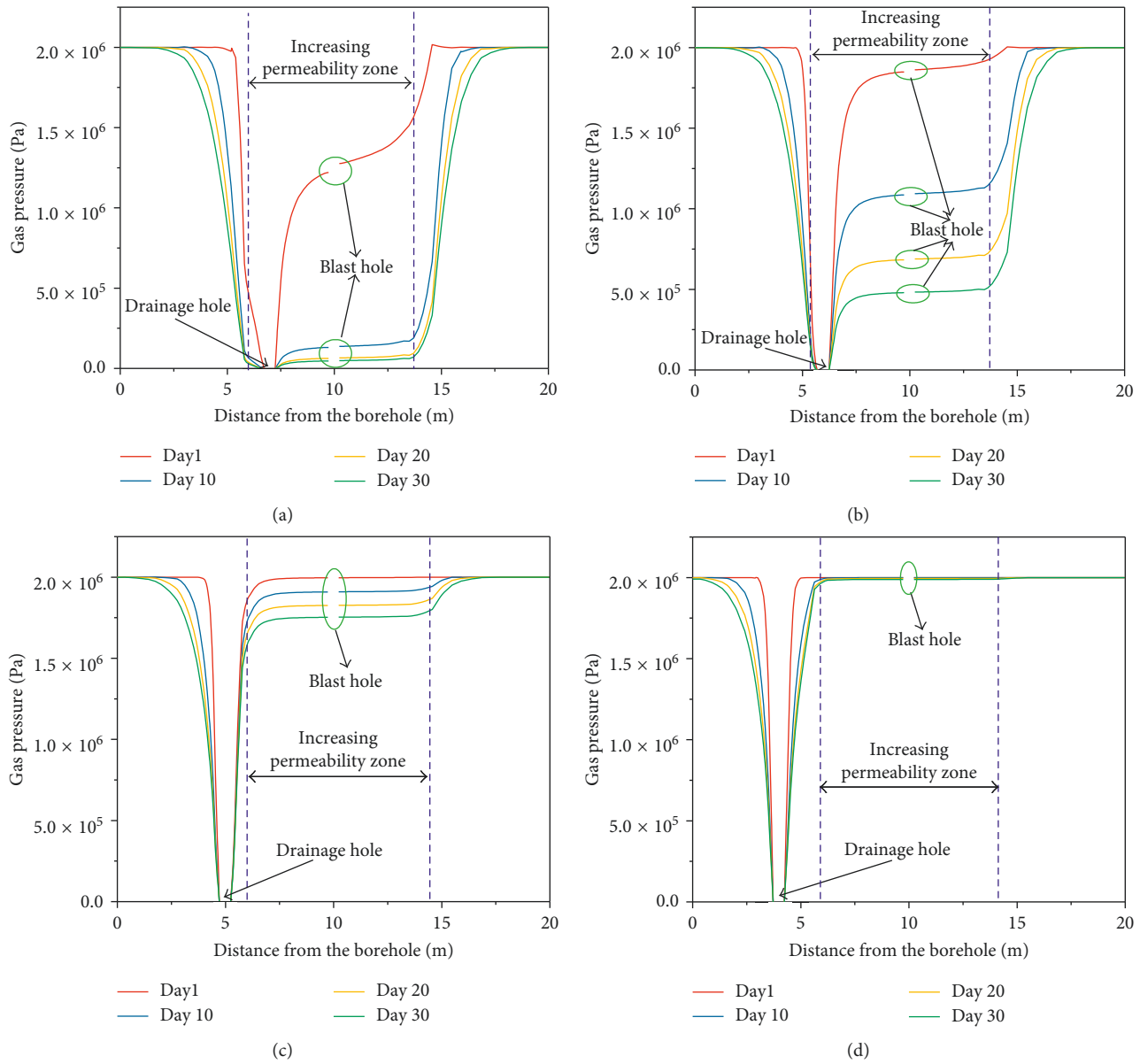

Figure 14: Variations of gas pressure as a function of time: (a) borehole spacing between the drainage hole and the blast hole is 3 m; (b) borehole spacing is 4 m; (c) borehole spacing is 5 m; (d) borehole spacing is 6 m.

hole are 4 and 5 m, respectively. The gas drainage hole at a spacing of 6 m is outside the increasing permeability zone. Therefore, after 30 d of gas drainage, the pressures in the coal of the increasing permeability zone are not effectively reduced. According to the above discussions, it can be seen that a reasonable spacing for effective gas drainage from the increasing permeability coal zone should be less than 5 m.

5. Field Test

5.1. Borehole Arrangements. Based on the numerical analysis results, the borehole arrangements in the test area are shown in Figure 15. All boreholes are divided into groups 1 and 2. In group 1, holes A and D are blast holes, and the even numbers (A2, A4, A6, and A8) around the blast hole A are drilled such that they are 3 m away from the blast hole. The odd number gas drainage holes (A1, A3, A5, and A7) are 4.2 m away from the blast hole A. Even numbers (D2, D4, D6, and D8) around the blast hole D are drilled at a distance of 5 m, and the odd-numbered gas drainage holes (D1, D3, D5, and D7) are 7 m away from the blast hole D. The borehole arrangements and spacings of group 2 are exactly the same as those of group 1.

5.2. Result Analysis. Figure 16 presents the average gas drainage flows for each spacing (3, 4.2, 5, and 7 m) in the cases of groups 1 and 2. As shown in Figure 16(a), after the application of LCDPTET, in group 1, the average flows of the gas drainage with 3, 4.2, 5, and 7 m before the explosion changed by a factor of 3.12, 1.91, 1.56, and 1.15, respectively, after explosion. In group 2, the average flows of gas drainage

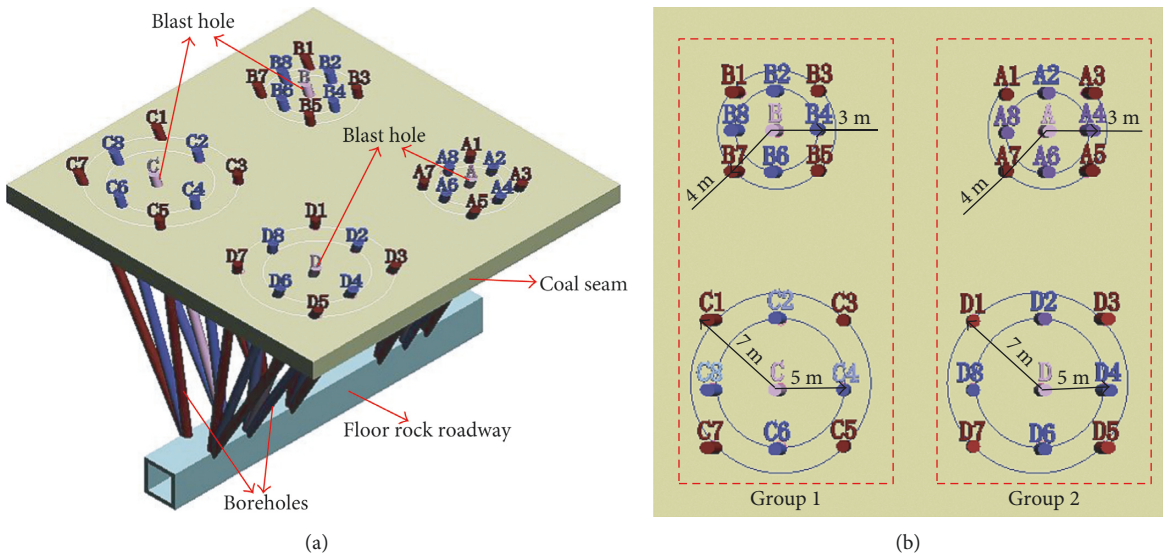

Figure 15: Borehole arrangements: (a) three-dimensional diagram; (b) top view.

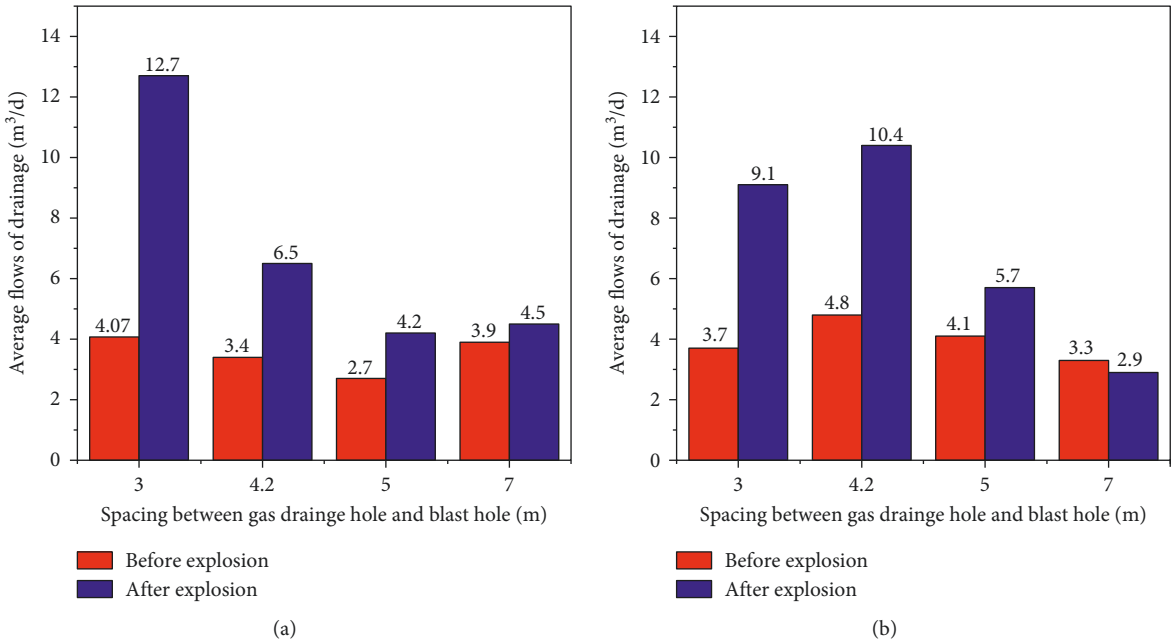

Figure 16: Average flows of gas drainage: (a) group 1; (b) group 2.

with spacings of 3, 4.2, 5, and 7 m before the explosion are increased by a factor of 2.46, 2.17, 1.39, and 0.88, respectively, after the explosion, as shown in Figure 16(b). After the explosion, the average flows of gas drainage in the cases where the borehole spacing ranged between 3 and 4 m boreholes are approximately twice the values attained before the explosion, which indicates that the permeability of the coal within a radius of 4 m around the blast hole is greatly improved. Gas drainage flows exhibit minor increases after the explosion at a spacing of 5 m. However, when the spacing is 7 m, comparison of the average flows of gas drainage before explosion with those after the explosion indicates that the gas drainage flows have not changed. Thus, the increasing permeability radius is approximately 5 m after the application of LCDPTET.

According to the field test, the closer the gas drainage hole is to the blast hole, the better are the gas drainage effects. However, it can be observed from the numerical simulation that when the gas drainage hole is 2 m away from the blast hole, the gas drainage hole will be located in the crushing zone where the coal is severely damaged. Thus, the gas drainage hole is prone to collapse and will affect the gas drainage efficiency. At the same time, small borehole spacing increases the drilling cost and construction time. Therefore,

considering the gas extraction efficiency, construction cost, and construction time comprehensively, the best spacing between the gas drainage hole and the blast hole is in the range of 3-4 m.

6. Conclusions

This study presented a new physical explosive technology (LCDPTET) to increase the permeability of high-gas and low-permeability coal seams and improve the gas drainage effects. The working principles of LCDPTET and its advantages of low-temperature, safety, and high efficiency were also illustrated. This study conducted at Qianxi county in the Guizhou province of China aimed at eliminating the risks of coal and gas outburst in roadway excavations, increasing coal permeability, improving gas drainage efficiency, and eliminating gas dynamic disasters. The following conclusions are drawn:

(1) A numerical model was built, and the damage index M_i was introduced to analyze the degree of coal damage by LCDPTE. According to the degree of coal damage, the damage zone was divided into crushing and fracture zones. Additionally, it was concluded that when there was only a single blast hole in the coal seam and the gas impact pressure was applied on the coal, the damage radius of the coal was 4.56 m. When there was a blast hole and a gas drainage hole in the coal seam at the same time, the damage radius of coal was about 5 m because the gas drainage hole provided a free surface for the deformation and expansion of the coal during the explosion. After the explosion, the coal permeability of the crushing zone increased from the initial value of $3.9 \times 10^{-16}\,\mathrm{m}^2$ to a value in the range of 7.2×10^{-13}–$1.14 \times 10^{-12}\,\mathrm{m}^2$, and the permeability in the fracture zone increased to a value in the range of 4.0×10^{-16}–$7.2 \times 10^{-13}\,\mathrm{m}^2$.

(2) Comparing the gas drainage effects of four different spacings between the gas drainage hole and the blast hole after the permeability of coal was increased by LCDPTE, it was observed that the gas pressures in the coal seams reduced considerably, and the gas drainage ranges were larger when the borehole spacings were 3 and 4 m. Under the premise that the boreholes would not collapse, a reasonable spacing between the blast hole and gas drainage hole was 3-4 m from the comprehensive considerations of the construction cost, construction time, and gas drainage effects.

(3) Field tests were conducted to investigate the increasing permeability range and gas drainage effect after the application of LCDPTE. In group 1, the average gas drainage flows for spacing of 3, 4.2, 5, and 7 m before explosion were modified by factors of 3.12, 1.91, 1.56, and 1.15, respectively, after explosion. In another group, the average gas drainage flows before the explosion were modified by factors of 2.46, 2.17, 1.39, and 0.88, respectively, after explosion. Therefore, the radius of the increasing permeability zone of coal is approximately 5 m. This also indicates that LCDPTE can effectively improve gas drainage efficiency.

Data Availability

The research data used to support the findings of this study are included within the article. Request for more details should be made to the corresponding author.

Conflicts of Interest

The authors declare no conflicts of interest.

Authors' Contributions

Wenrui He performed the technological development and the program design and prepared and edited the manuscript. Fulian He revised and reviewed the manuscript. Kun Zhang, Yongqiang Zhao, and Hengzhong Zhu proofread the manuscript.

Acknowledgments

This work was supported by National Natural Science Foundation of China (Grant no. 51574243), the Fundamental Research Funds for the Central Universities (Grant no. 800015J6), and the Yue Qi Distinguished Scholar Project, China University of Mining and Technology, Beijing (Grant no. 800015Z1138).

References

[1] S. N. Zhou, "Mechanism of gas flow in coal seams," *Journal of China Coal Society*, vol. 15, no. 1, pp. 15–24, 1990.

[2] M. G. Qian, X. X. Miao, and J. L. Xu, "Green mining of coal resources harmonizing with environment," *Journal of China Coal Society*, vol. 32, no. 1, pp. 1–7, 2007.

[3] C. Zhai, B. Q. Lin, and L. Wang, "Status and problems of drainage and utilization of downhole coalbed methane in coal mines in China," *Natural Gas Industry*, vol. 28, no. 7, pp. 23–26, 2008.

[4] M. F. Romeo, "Coalbed methane: from hazard to resource," *International Journal of Coal Geology*, vol. 35, pp. 13–26, 2013.

[5] J. Yun, F. Y. Xu, L. Liu et al., "New progress and future prospects of CBM exploration and development in China," *International Journal of Mining Science and Technology*, vol. 22, no. 3, pp. 363–369, 2012.

[6] C. Boger, J. S. Marshall, and R. C. Pilcher, "Worldwide coal mine methane and coalbed methane activities," in *Coal Bed Methane: from Prospect to Pipeline*, pp. 351–407, Elsevier, New York, NY, USA, 2014.

[7] D. Greedy and H. Tilley, "Coalbed methane extraction and utilization," *Journal of Power and Energy*, vol. 217, no. 1, pp. 19–26, 2003.

[8] C. O. Karacan, F. A. Ruiz, M. Cote et al., "Coal mine methane: a review of capture and utilization practices with benefits to mining safety and to green-house gas reduction," *International of Journal Coal Geology*, vol. 86, no. 2-3, pp. 121–156, 2011.

[9] B. Liang, X. P. Yuan, and W. J. Sun, "Seepage coupling model of in-seam gas extraction and its applications," *Journal of*

China University of Mining and Technology, vol. 43, no. 2, pp. 208–213, 2014.

[10] H. P. Xie, F. Gao, H. W. Zhou et al., "On theoretical and modeling approach to mining-enhanced permeability for simultaneous exploitation of coal and gas," *Journal of China Coal Society*, vol. 38, no. 7, pp. 1101–1108, 2013.

[11] W. C. Wang, X. Z. Li, B. Q. Lin et al., "Pulsating hydraulic fracturing technology in low permeability coal seam," *International Journal of Mining Science and Technology*, vol. 25, no. 4, pp. 681–685, 2015.

[12] J. Liu, Z. G. Liu, J. H. Xue et al., "Application of deep borehole blasting on fully mechanized hard top-coal pre-splitting and gas extraction in the special thick seam," *International Journal of Mining Science and Technology*, vol. 25, no. 5, pp. 755–760, 2015.

[13] G. Z. Hu, H. T. Wang, X. G. Fan et al., "Mathematical model of coalbed gas flow with Klinkenberg effects in multi-physical fields and its analytic solution," *Transport Porous Media*, vol. 76, no. 3, pp. 407–420, 2009.

[14] G. Z. Hu, X. Huang, J. L. Xu et al., "A co-extraction technology of coal and CBM base on the law of gas advanced relieving pressure of in-seam coalface," *Disaster Advance*, vol. 5, no. 4, pp. 867–872, 2012.

[15] G. Z. Hu, J. L. Xu, T. Ren et al., "Adjacent seam pressure-relief gas drainage technique based on ground movement for initial mining phase of longwall face," *International Journal of Rock Mechanics and Mining Science*, vol. 77, pp. 237–245, 2015a.

[16] G. Z. Hu, X. Huang, and J. L. Xu, "Effect of microwave field on pore structure and absorption of methane in coal," *Journal of China Coal Society*, vol. 40, no. S2, pp. 374–379, 2015.

[17] S. P. Singh, "Non-explosive applications of the PCF concept for underground excavation," *Tunnelling and Underground Space Technology*, vol. 13, no. 3, pp. 305–311, 1998.

[18] M. G. Jaimes, R. D. Castillo, and S. A. Mendoza, "High energy gas fracturing: a technique of hydraulic prefracturing to reduce the pressure losses by friction in the near wellbore - A Colombian field application," in *Proceedings of SPE Latin American and Caribbean Petroleum Engineering Conference Proceedings*, vol. 2, pp. 919–930, Lima, Peru, April 2012.

[19] F. P. Wu, X. M. Wei, Z. X. Chen et al., "Numerical simulation and parametric analysis for designing High Energy Gas Fracturing," *Journal of Natural Gas Science and Engineering*, vol. 53, pp. 218–236, 2018.

[20] X. Anon, "Carbon system brings benefits in the mining of large coal," *Coal International*, vol. 243, pp. 27-28, 1995.

[21] N. Vidanovic, S. Ognjanovic, N. Ilincic et al., "Application of unconventional methods of underground premises construction in coal mines," *Technics Technologies Education Management (TTEM)*, vol. 6, pp. 861–865, 2011.

[22] Z. S. Du, Y. C. Fan, Y. F. Xue et al., "Study on carbon dioxide blasting mining and driving equipment and technology," *Coal Science and Technology*, vol. 9, no. 44, pp. 36–42, 2016.

[23] K. M. Sun, L. W. Xin, T. T. Wang et al., "Simulation research on law of coal fracture caused by supercritical CO_2 explosion," *Journal of China University of Mining and Technology*, vol. 46, no. 3, pp. 501–506, 2017.

[24] H. D. Chen, Z. F. Wang, X. E. Chen et al., "Increasing permeability of coal seams using the phase energy of liquid carbon dioxide," *Journal of CO_2 Utilization*, vol. 19, pp. 112–119, 2017.

[25] W. B. Sun and Y. Wang, "Numerical simulation of rock fracturing by carbon dioxide phase transition," in *Proceedings of Mechanics Symposium*, vol. 3, pp. 1962–1967, Ostrava, Czech Republic, June 2017.

[26] H. Z. Wang, G. S. Li, Z. G. He et al., "Mechanism study on rock breaking with supercritical carbon dioxide jet," *Atomization and Sprays*, vol. 27, no. 5, pp. 383–394, 2017.

[27] L. H. Jiang, M. B. Wang, and M. Zhang, "Application and advantages of high energy gas fracturing at home and abroad," *Petrochemical Industry Application*, vol. 3, no. 35, pp. 7–9, 2017.

[28] X. M. Sun, *Research on Strengthening Gas Pre-Drainage Effect with the Fracturing Technique by Liquid CO_2 Phase Transition in Layer through Boring*, Henan Polytechnic University, Henan, China, 2014.

[29] M. Xu, *Research of Liquid CO_2 Phase Transition Fracturing Technology in Coal Seam*, Henan Polytechnic University, Henan, China, 2016.

[30] SY/T 5336–2006, *Practices for Core Analysis*, China Petroleum Industry Standard, China, 2006.

[31] GBT–19560–2008, *Experimental Method of High-Pressure Isothermal Adsorption to Coal*, China National Standard, China, 2008.

[32] GB/T 23250–2009, *The Direct Method of Determining Coalbed Gas Content in the Mine*, China National Standard, China, 2009.

[33] AQ/T 1047–2007, *The Direction Measuring Method of the Coal Seam Gas Pressure in Mine*, China Industry Standard Concerning Safety Production, China, 2007.

[34] W. C. Zhu, C. H. Wei, J. Tian et al., "Coupled thermal-hydraulic-mechanical model during rock damage and its preliminary application," *Rock and Soil Mechanics*, vol. 12, no. 30, pp. 1253–1263, 2009.

[35] M. A. Biot and D. G. Willis, "The elastic coefficients of the theory of consolidation," *Journal of Applied Mechanics-Transactions*, vol. 24, pp. 594–601, 1957.

[36] J. Rutqvist and C. F. Tsang, "A study of cap rock hydromechanical changes associated with CO_2-injection into a brine formation," *Environmental Geology*, vol. 42, no. 2-3, pp. 296–305, 2002.

[37] E. Y. Wang, X. G. Kong, and S. B. Hu, "Multi-scale fractured coal gas-solid coupling model and its application in engineering projects," *Transport in Porous Media*, vol. 121, no. 3, pp. 703–724, 2018.

[38] G. Z. Hu, H. T. Wang, X. G. Fan et al., "Investigation on law of methane gas flow in coal with coal-gas outburst hazard and low permeability," *Chinese Journal of Rock Mechanics and Engineering*, vol. 12, no. 28, pp. 2528–2534, 2009.

[39] N. Mohammad, D. J. Reddish, and L. R. Stace, "The relation between in situ and laboratory rock properties used in numerical modeling," *International Journal of Rock Mechanics and Mining Science*, vol. 34, no. 2, pp. 289–297, 1997.

[40] M. F. Cai, M. C. He, and D. Y. Liu, *Rock Mechanics and Engineering*, Science Press, Bejing, China, 2nd edition, 2013.

[41] W. C. Zhu, C. N. Tang, T. H. Yang et al., "Constitutive relationship of mesoscopic elements used in $RFPA^{2D}$ and its validations," *Chinese Journal of Rock Mechanics and Engineering*, vol. 22, no. 1, pp. 24–29, 2003.

[42] J. J. Chen and F. S. Zhou, "The change of rock permeability with high energy underground explosion," in *Proceedings of 5th China Engineering Geology Conference*, pp. 203–207, Beijing, China, 1996.